Hacıoğlu *et al. Earth, Planets and Space (2018) 70:161*
https://doi.org/10.1186/s40623-018-0932-3

Earth, Planets and Space

FULL PAPER Open Access

Crustal structure of a young collision zone: the Arabia–Eurasia collision in northeastern Turkey investigated by magnetotelluric data

Özlem Hacıoğlu[1,2*], Ahmet Tuğrul Başokur[3] and Elif Tolak Çiftçi[1]

Abstract

The northeastern Turkey is located at the intensely deformed east Anatolian Collision Zone that is formed by the collision of the Arabian Plate with Eurasia. The region is one of the best examples of the continental collision zone in the world and exhibits an active north–south shortening and a young and widespread volcanism. In northeastern Anatolia, the ongoing motions of the Arabian and Eurasian Plates through a range of deformation processes have generated the Erzurum–Kars Plateau, a region of large-scale deformation and uplift observed at surface. However, the nature of deformation driven by the continental collision remains unresolved at depth. In this study, magnetotelluric (MT) data recorded at 74 sites constituting two intersecting profiles have been used to construct the characteristic electrical conductivity pattern associated with the intensely deformed east Anatolian Collision Zone beneath the Erzurum–Kars Plateau, northeastern Turkey, with the aim of imaging the 3D distribution of fluids in order to link it with subsurface rheological conditions. An equal number of colocated transient electromagnetic (TEM) sounding data were used to allow the static shift correction of the MT data; a borehole was also drilled inside the study area. We ran a one-dimensional inversion of TEM data in order to determine shift in MT data and a three-dimensional inversion using full components of MT impedance tensor previously corrected for static shift. The resulting models showed that two distinct conductive zones probably indicating local accumulation of melt exist at mid-to-lower crustal depths (15–45 km) throughout the Erzurum–Kars Plateau. The spatial distribution of these anomalously conductive zones mechanically characterizes weak areas that may permit flow of crustal materials in the collision zone. These conductive zones have been previously identified further west of the collision zone, which implies that the electrical characteristic of the collision zone is continuous from west to east beneath the Anatolian Plateau. The spatial extent of the conductive zones may suggest the presence of two localized crustal flow channels situated laterally parallel to the orogeny. These findings can potentially contribute to understanding of the crustal structure of collision zones, in particular east Anatolian Collision Zone, and the hypothesis that crustal flow can occur in orogenic belts.

Keywords: Continent–continent collision, Eastern Anatolia, Erzurum–Kars Plateau, Anatolian Plateau, 3D inversion, Magnetotellurics, Electrical conductivity, Crustal fluids, Rheology

Introduction

Continent–continent collisions are invaluable records to explain the tectonic evolution of the Earth and thus have always been interesting for Earth scientists. Eastern Anatolia is regarded as one of the two largest regions in the world in which an active continent–continent collision is currently occurring. The other one is the Tibetan Plateau and Himalaya which has been formed by the India–Asia collision. On the other hand, the Arabia–Eurasia collision has formed Eastern Anatolia, namely the Anatolian–Iranian Plateau (Şengör and Kidd 1979; Dewey et al. 1986). The Anatolian–Iranian Plateau in many aspects such as topographic uplift and young volcanism resembles the Tibetan Plateau, and thus, it has been viewed as a younger version of the Tibetan Plateau in many studies

*Correspondence: ozlem.cengiz@boun.edu.tr
[1] Geophysics Department, Kandilli Observatory and Earthquake Research Institute, Boğaziçi University, 34684 Çengelköy, Üsküdar, Istanbul, Turkey
Full list of author information is available at the end of the article

(e.g., Şengör and Kidd 1979; Dewey et al. 1986). The Arabia–Eurasia collision in Eastern Anatolia began around 13 Ma (Dewey et al. 1986), while the age of the collision between India and Asia extended from 50–55 to 70 Ma (Aitchison et al. 2007).

The Arabian–Eurasian collision zone is a spectacular region to study the early stages of a continent–continent collision zone, and a number of geological and geophysical studies have been performed to examine the crust and upper mantle structure beneath Eastern Anatolia in order to constrain the nature of the collision. Receiver function studies in Eastern Anatolia suggest various crustal low velocity zones that have been associated with partial melt in the mid crust (Angus et al. 2006). Low Pn velocities (Al-Lazki et al. 2003), shear wave velocities (Gök et al. 2007; Maggi and Priestley 2005) and Sn attenuation (Al-Damegh et al. 2004; Barazangi et al. 2006) indicate that the uppermost mantle is partially molten. High Bouguer gravity anomalies in Eastern Anatolia also indicate that the crust floats on a partially molten asthenosphere (i.e., there is no lithospheric mantle), and the asthenospheric material is therefore in direct contact with the base of the crust (Ateş et al. 1999; Barazangi et al. 2006). The absence of subcrustal earthquakes (Türkelli et al. 2003) indicates that the underthrusting of Arabian Plate beneath Eurasia is either very little or totally absent. The strike-slip characteristic of crustal seismicity in Eastern Anatolia also indicates that the northward convergence of Arabian Plate is accommodated by tectonic escape (Örgülü et al. 2003), and the topographic uplift supported by emplacing hot asthenosphere at subcrustal depths provides slab detachment in Eastern Anatolia (Şengör et al. 2003; Keskin 2003).

Magnetotelluric (MT) imaging of the crustal and upper mantle structures in collision zones plays a crucial role in defining their present-day structure and tectonic evolution since the fluid content and thermal structure, which are the most critical parameters for characterizing the rheology of the crust and upper mantle, can be constrained with the help of MT data (Unsworth 2010). The regional-scale MT study in Eastern Anatolia was carried out by Türkoğlu et al. (2008, 2015), Türkoğlu (2009) and Avşar et al. (2013). Türkoğlu et al. (2008) used long-period MT data obtained from two main profiles in order to image the conductivity structure of the region. The electrical conductivity models derived from two-dimensional (2D) inversion of MT data revealed the high-conductivity pockets interpreted as an indication of local accumulation of melt in the crust of the Anatolian Plateau. In this study, we also used the MT method in order to detect the presence of fluids or melt in the crust of the east Anatolian Collision Zone. We specifically focused on the northern part of the collision zone, the Erzurum–Kars Plateau (EKP) (Fig. 1) in order to generate the first three-dimensional (3D) conductivity model for the region, and also based on this model, we linked the distribution of fluids with subsurface rheology. Furthermore, we aimed to image whether the conductive zones previously documented by Türkoğlu et al. (2008) continue eastward in the crust of the collision zone and to give an additional contribution to the idea that localized crustal flow may occur in east Anatolian Collision Zone (Türkoğlu et al. 2008; Unsworth 2010).

Tectonic and geologic setting

The collision between the Eurasian and Arabian Plates in the Middle Miocene, after the subduction of the Neo-Tethys Ocean beneath Eurasia (Dewey et al. 1986; Şengör and Yılmaz 1981), formed Eastern Anatolia and its present-day tectonics. Many geodynamic models have been suggested and discussed in order to explain the evolution of the collisional zone. Some models proposed that the Anatolian Plateau was formed by the Arabian Plate convergence being accommodated by lithospheric thickening (Dewey et al. 1986) or tectonic escape (McKenzie 1972), whereas others asserted that it resulted from the continental subduction (Rotstein and Kafka 1982), lithospheric delamination (Pearce et al., 1990), slab detachment (Innocenti et al. 1982) or slab steepening and break-off beneath a large subduction–accretional complex (Şengör et al. 2003; Keskin 2003; Barazangi et al. 2006). The distribution of collision-related volcanic units across Eastern Anatolia characterizes deep delamination model (Pearce et al. 1990; Keskin et al. 1998) and the asthenospheric mantle in contact with the accretionary complex at shallow depths (~ 50 km) as a result of slab steepening and break-off beneath the subduction–accretional complex (Keskin 2003). Today, the ongoing northward motion of the African and Arabian Plates with respect to the Eurasian Plate is accommodated in large part by lateral transport within the interior part of the collision zone and lithospheric shortening and thickening along the Caucasus and Zagros mountain belts (Reilinger et al. 2006).

The continental collision between the Arabian and the Eurasia Plates in Eastern Anatolia resulted in a tectonic collage including different microcontinents separated by ophiolithic belts and accretionary complexes (Keskin et al. 2006) (Fig. 1). These tectonic blocks are known as the Rhodope-Pontide fragment, the Northwest Iranian fragment, the East Anatolian Accretionary Complex (EAAC) and the Bitlis-Pötürge Massif (Şengör et al. 2003; Keskin 2003). The Rhodope-Pontide fragment is characterized by an ensialic, south-facing magmatic arc (Şengör et al. 2003), and it is formed by north-dipping subduction under the Eurasian Plate in a period between the

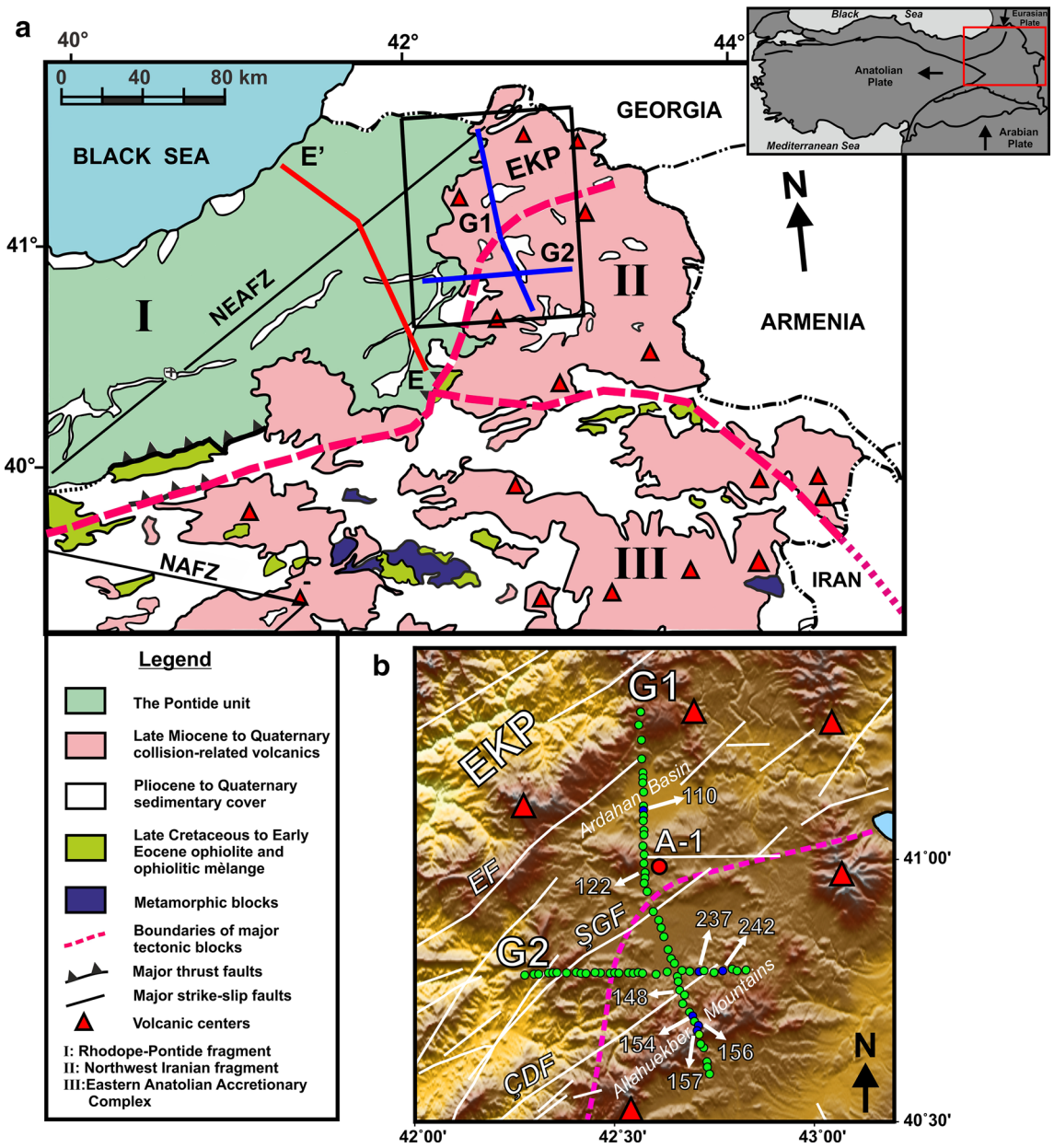

Fig. 1 **a** Simplified geological map and tectonic blocks (modified from Şengör et al. 2003; Keskin et al. 2006; Keskin 2005) showing the study area (black rectangular box) with MT profiles (blue solid lines, G1 and G2). Red solid line (E′-E) denotes approximate location of the MT profile from previous study by Türkoğlu et al. (2008). **b** Topographic map of Erzurum–Kars Plateau superposed with fault branches (white solid lines). Yellow dots show the location of MT sites. Blue dots show the location of MT sites distorted by static shift. Red dot indicates position of the borehole (A-1). EKP: Erzurum–Kars plateau, NEAFZ: Northeast Anatolian fault zone, NAFZ: North Anatolian fault zone, ÇDF: Çobandede fault, EF: Erzurum fault, ŞGF: Şenkaya–Göle fault

Albian and Oligocene times (Yılmaz et al. 1997; Şengör et al. 2003). The Northwest Iranian fragment is masked by collision-related volcanic units in Eastern Anatolia, and it consists of heterogeneous rocks (Keskin 2005). The EAAC represents a huge subduction–accretion complex located between the Rhodope-Pontide fragment and Bitlis-Pötürge Massif, and it is composed of late Cretaceous or much younger ophiolitic mélange and Paleocene to late Oligocene flysch sequences (Şengör et al. 2003). The EAAC has a special significance due to the fact that it has been exposed to a high collision-related magmatic activity and accommodating most of deformation driven

by the continental collision (Keskin 2003). The Bitlis-Pötürge Massif is an intensely deformed metamorphic massif which is allochthonous on late Cretaceous and medial Eocene mélange complex (Şengör et al. 2003).

The neotectonic structure in Eastern Anatolia is dominated by roughly north–south convergence between the Arabian and Eurasian Plates (Bozkurt 2001). The dominant and active structural elements of the region are the NE–SW- and SE–NW-trending strike-slip faults and fewer east–west-trending thrust faults (Bozkurt 2001; Şengör et al. 2003; Örgülü et al. 2003). Among these faults, the Northeast Anatolian fault zone is one of the most important elements in Eastern Anatolia (Fig. 1), and it is an approximately 350-km-long left-lateral strike-slip fault zone extending from the Erzincan basin to the Great Caucasus (Bozkurt 2001). The east–west-trending pull-apart basins, which are originated by the compressional tectonic regime of the region, have developed along these fault systems and undeformed Pliocene to Quaternary continental volcano-sedimentary sequences accumulated in some basins (Bozkurt 2001; Koçyiğit et al. 2001). The north–south-trending fissures filled with magma and associated Pliocene to Quaternary volcanoes are the other structural elements of the region (Bozkurt 2001; Koçyiğit et al. 2001). Although volcanic units cover over half of the region in Eastern Anatolia, in the north around the EKP, volcanic units have a special importance due to containing a more complete record of volcanism from middle Miocene to Pliocene (Keskin et al. 1998, 2006).

MT and TEM data

The MT and TEM measurements in the EKP were taken to depict subsurface electrical conductivity structure of Eastern Anatolia. A total of 74 MT soundings have been acquired in the survey. The wideband MT data were collected at two intersecting profiles. The first profile (G1) consists of 44 MT sites along the ~ 80-km-long nearly north–south profile, and the second (G2), east–west-trending profile is composed of 30 MT sites along the ~ 50-km-long profile (Fig. 1). Five-component MT data (Ex, Ey, Hx, Hy and Hz) were acquired using Metronix ADU-06 MT data acquisition systems using non-polarizing Pb–$PbCI_2$ electrodes with dipole lengths 50–100 m and three induction coils (EMI BF-4 and BF-7). At each site, ~ 15 h of recording was made covering a period range from 0.03 to 1000 s with a remote reference site. The measured time series were processed in two steps, which are the single-site processing and remote reference processing, using the robust code developed by Larsen et al. (1996). The remote reference technique was applied in order to enhance the data quality (Gamble et al. 1979). The same number of central loop transient electromagnetic (TEM) soundings with MT soundings was collected at colocated sites with the aim of providing a natural remedy for the MT static shift (Pellerin and Hohmann 1990). A Zonge GDP-32 EM data logger and a transmitter with current loop size of either 100×100 or 150×150 m^2 depending on terrain limitations were used to obtain TEM data. A receiver coil was positioned in the center of the transmission loop to measure the decay of the secondary magnetic field. The transmitter square wave current ranged from 9 to 20 A at repetition frequencies of 8 and 2 Hz. The measured TEM data were processed using the interpretation package TEMIXXL manufactured by Interpex (1996) in order to calculate late-time apparent resistivity as a function of time. The voltage decay curves were evaluated to determine the asymptotic (late time) noise levels, and the data points at or close to this level (1–10 nV/Am^2) were removed prior to merging of multiple runs and subsequent interpretation. We utilized one-dimensional (1D) inversion based on the dumped least squares inversion algorithm for horizontal layers (ridge regression) to describe the number of layers, their thicknesses and conductivity of each layer.

Static shift correction

Theoretically, galvanic distortions in 3D modeling would not be a problem if the measured MT data were well modeled to resolve all inhomogenities (Jones 2012). However, this leads to excessive computational load. This type of distortion caused by local, near surface inhomogenities in a 1D or 2D regional structures is independent of the frequency, while if the regional structure is 3D, its effect on measured data becomes frequency dependent. Hence, both apparent resistivity and phase responses are disturbed by a frequency-dependent term (Ledo et al. 1998). Thus, a correction should be performed prior to 3D interpretation in order to retrieve information about the regional 3D structure. To correct galvanic distortions (except the static shift), we applied a 3D galvanic distortion model over 3D regional structure proposed by Ledo et al. (1998) for retrieval of the regional transfer functions. Accordingly, we applied the Groom and Bailey (GB) decomposition (Groom and Bailey 1989) for the short periods at each site in order to determine distortion parameters, namely twist and shear. The calculated value of these parameters is approximately 0 degree for almost all sites, which implies that the measured MT data are not distorted by corresponding galvanic effects, and therefore, the data have not been corrected from such distortions prior to inversion. On the other hand, static shift, which is another galvanic distortion effect that shifts apparent resistivity curves by a scaling factor while keeping the phases unchanged and independent of the frequency, was corrected by utilizing a 1D inversion of TEM

data since the TEM data are relatively not affected by near surface inhomogenities. Figure 2a shows an example of static shift effect on off-diagonal components of the impedance tensor (Z_{xy} and Z_{yx}) intriguingly splitting at high frequencies at a MT site (110) by comparing with the transient apparent resistivity curve, which is probably due to a combination of the mountainous topography of the EKP and surficial inhomogeneities. However, the on-diagonal components of impedance tensor (Z_{xx} and Z_{yy}) at short periods (< 0.1 s) show one-dimensional structure with its small values, which indicates that the on-diagonal components are not affected by static shift, and therefore, a static shift correction was not applied to these components. The effect of static shift on the components of impedance tensor shows similar characteristic at all those sites affected by this type of distortion. To achieve the static shift correction, we followed a correction procedure to shift distorted MT curves to their correct values based on 1D inversion of colocated TEM data and thus eliminated static shifts at six sites. Five of these sites are located on collision-related volcanics in the Northwest Iranian fragment; particularly, three of them are situated in the vicinity of the Allahuekber Mountains, and one is located near the Ardahan pull-apart basin in the Rhodope-Pontide fragment (Fig. 1). Since it is only an assumption that the earth beneath a TEM current ring is 1D, the phases of the measured impedances were rotated to 45° in order to show that the data are 1D at short periods (Fig. 2b). The dimensionality parameters (phase tensor beta values) also indicate 1D behavior for short periods (Fig. 3), and when we compared the data with the data from neighboring sites, the distortion at corresponding sites is obvious. Figure 2c shows corrected apparent resistivity curves, and Fig. 2d displays inverted layered earth models corresponding to TEM sounding data and shifted MT data for the exemplary site. The estimated resistivity distribution with depth for the site affected by static shift and corrected for the shift clearly shows that the static shift effect may lead to incorrect estimations of resistivities and thus erroneous modeling of subsurface electrical conductivity structure as a result of misinterpretation of measured MT data.

Dimensionality

Prior to the inversion of MT data, the dimensionality and the directionality of the data were examined through phase tensor analysis (Fig. 3). The attraction of this approach is to provide the distortion-free dimensionality information without any assumptions about the dimensionality of the regional response tensor in the existence of electric field galvanic distortion (Caldwell et al. 2004; Jones 2012; Booker, 2014). The spatial variations of the phase tensor ellipses provide information about localized conductivity changes in the subsurface (Ferguson et al. 2012). Therefore, it is advantageous to take into consideration the information containing phase tensor.

The phase tensor described by the relation between the real and imaginary parts of the impedance tensor can be represented graphically by an ellipse characterized by three invariants, the major and minor axes and skew angle (β). While the maximum and minimum phase difference between the horizontal components of the electric and magnetic fields is defined by the principle axes of the tensor, the asymmetry in the MT responses is represented by the phase tensor skew angle (Caldwell et al. 2004). The color of the ellipses representing the skew angle describes a measure of the dimensionality of the observed MT data, and the large values of it ($|\beta| > 3^{\circ}$) imply the existence of 3D regional conductivity structure (Caldwell et al. 2004; Booker 2014). Furthermore, the polarization direction of the ellipses shows the direction of the current flow, and inconsistent variation in the polarization directions of ellipses is also an indicator of 3D regional conductivity structure even if the value of beta is small (Caldwell et al. 2004). Figure 3 summarizes the results of the phase tensor analysis for both G1 and G2 profiles. Here, we used 95% confidence limit. The error of the phase tensor data was also taken into consideration, as suggested by Booker (2014). In order to estimate skew angle errors, ten thousand skew values were computed by utilizing different values of all components of impedance tensor (Z_{xx}, Z_{xy}, Z_{yx} and Z_{yy}) which are randomly distributed within the total range of the assumed error, following the approach of Campanyà et al. (2016). For periods smaller than 0.1 s, most of the ellipses show weak polarization and the small skew values (mostly < [− 2° 2°]), indicating that 1D or 2D structures are dominant. However, as period increases, the value of skew angle increases to greater values, which indicates 3D structures. The polarization direction of most of the ellipses exhibits a consistent trend with the geo-electric strike directions (N95°E for G1 and N110°E for G2 profiles), which is shown as rose diagrams and obtained using the MTpy python toolbox (Krieger and Peacock 2014), as being parallel to roughly north–south-trending compressional stresses associated with collision of the Arabian with Eurasia (Reilinger et al. 1997). Similarly, the multi-site–multi-frequency decomposition (McNeice and Jones 2001), an extended form of the GB decomposition yielded a geo-electric strike angle of N92°E for G1 and N100°E for G2 profiles, respectively. The shadow portions in the phase tensor pseudo-sections indicate the areas associated with mid-to-lower crustal conductive zones (C1 and C2), showing high beta values and ellipticities. Comparing skew angle values and associated errors at all sites and periods, we can suggest that

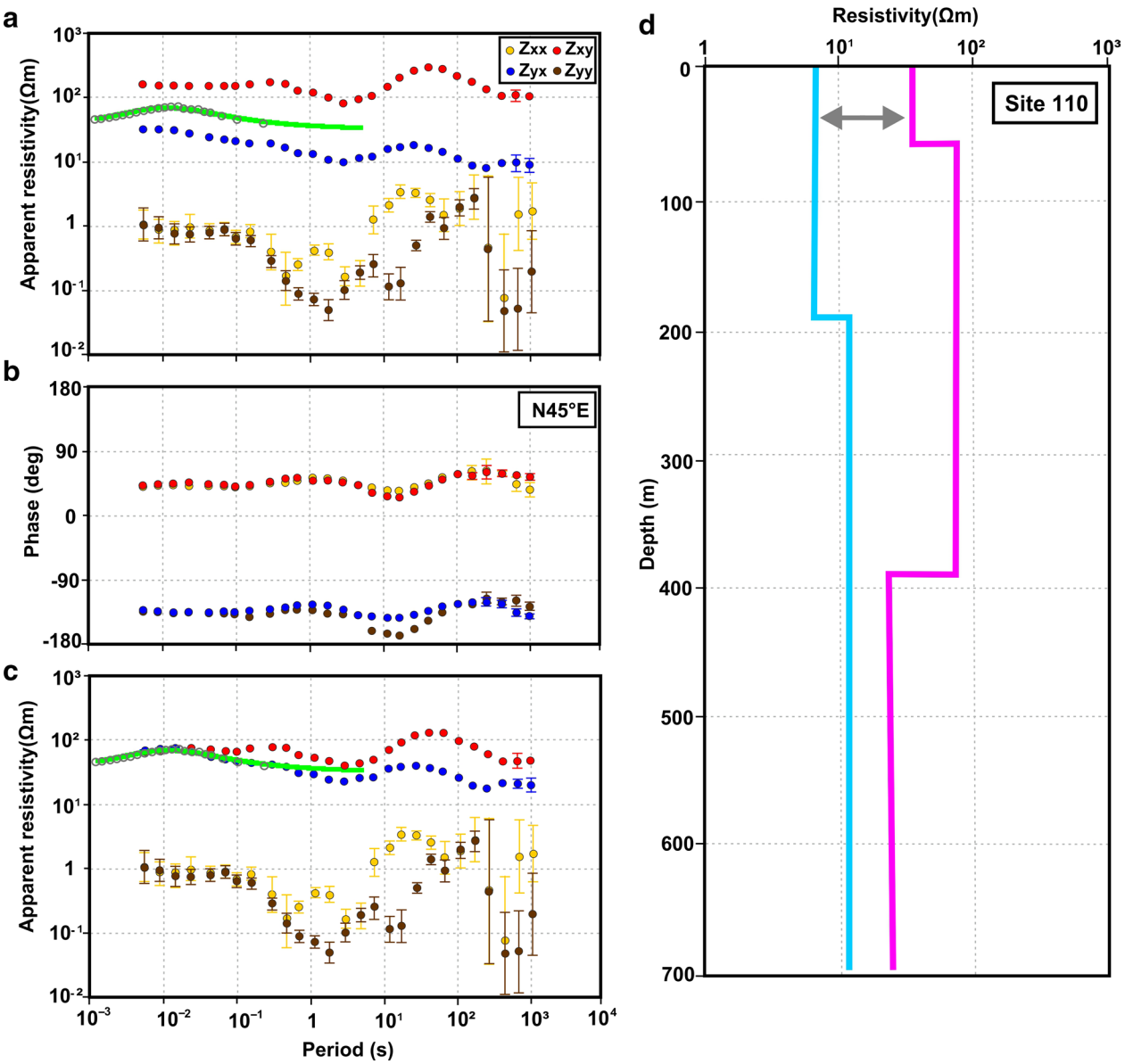

Fig. 2 MT static shift correction using the TEM data. **a** Comparison of the MT sounding curve with TEM sounding curve at site 110. **b** Phase of the 45° rotated MT sounding curves, showing that the curves are 1D at short periods. **c** Static shift-corrected MT sounding curves using 1D inversion of the central loop TEM data acquired at colocated site. **d** Comparison of the inverted 1D layered models corresponding to the TEM sounding data (pink) and shifted MT data (blue). Gray circles and green solid line are observed and calculated TEM data, respectively. The location of the site is shown in Fig. 1b

the phase tensor ellipses characterize a 3D environment with high beta and ellipticities and small error values at most of the sites. Therefore, the dominant 3D behavior of the data shown by phase tensor analysis requires a 3D interpretation.

Magnetotelluric inversion

MT data have been traditionally collected on 2D profiles across a geo-electric strike direction assumed from regional geology and then interpreted using 2D procedures, which are based on the rotation of the MT impedances into the determined geo-electric strike direction in order to fit off-diagonal impedances (TE and TM apparent resistivities and phases) for 2D inversion, together with treating the data from 3D complications. In the present study, our data were also collected on two intersecting individual profiles (Fig. 1), but 2D interpretation of data may result in unrealistic images of structure beneath

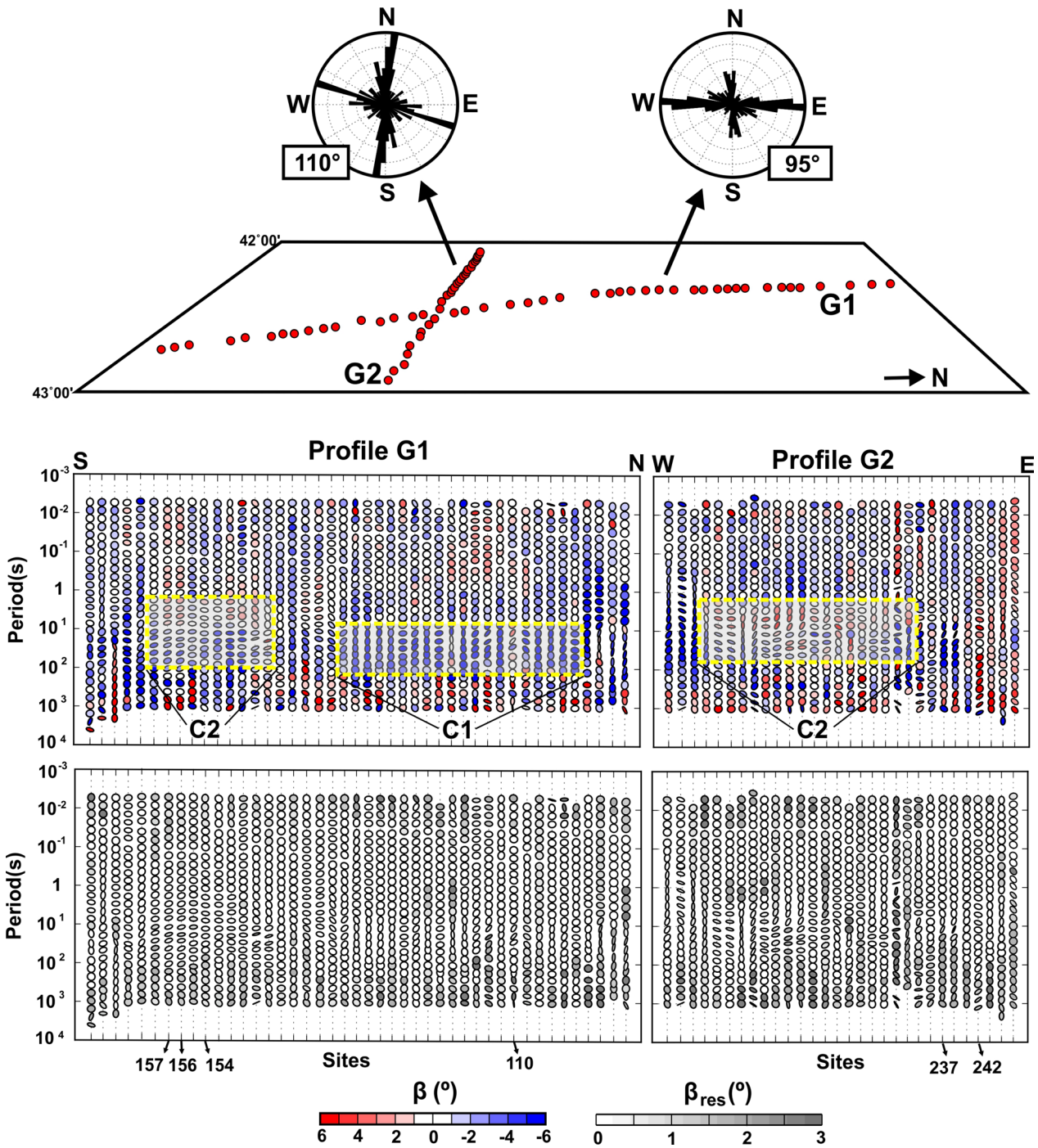

Fig. 3 Geo-electric strike directions and phase tensor ellipses for the whole data. Strike directions obtained by phase tensor analysis are shown as rose diagrams. The resolution of rose diagrams is 5 degrees. The phase tensor ellipses which are normalized by the major axes are filled with the skew angle (β) and residual of the skew angles (β_{res}). The yellow rectangles indicate high beta values, and ellipticities attributed to the mid-to-lower crustal conductive zones (C1 and C2)

the profiles because the dimensionality analysis suggests a 3D environment.

A study by Siripunvaraporn et al. (2005b) applied 3D inversions to synthetic data and demonstrated the advantageous of interpreting single-profile MT data with a 3D inversion algorithm. They suggested that the inversion of a single-profile MT data with a 3D inversion code produces significantly more realistic images of structures

beneath the profile, and also including the on-diagonal impedance elements in 3D inversion leads to a more meaningful model near the data transect as improving the accuracy of the images of off-profile structures. On the other hand, Patro and Egbert (2011) using real MT data from two profiles on the Deccan Volcanic Province discussed the advantage of modeling the single-profile MT data with the same 3D interpretation approach. They concluded that models obtained from 3D inversion fit the data better than the models produced by 2D inverse solutions, and while many of the features exist on models obtained from both 2D and 3D inversions, the amplitudes and positions of individual conductive features differ in some cases, particularly in the case of using the longer smoothing length scales along the geo-electric strike direction. Therefore, spatially correct location of off-profile structures and considerably more realistic images of structures beneath the profiles have motivated us to interpret single-profile MT data sets by a 3D inversion approach instead of a 2D inversion approach.

The 3D MT inversion algorithm WSINV3DMT was used to invert the MT data collected on two intersecting profiles G1 and G2. The code implements a 3D minimum structure inversion algorithm based on a data-space variant of the Occam approach (Siripunvaraporn et al. 2005a). Since 3D inversion is very expensive in terms of both computational time and storage, some compromises such as reducing the number of periods and using a relatively coarse grid were required when preparing the initial models and data. We used full components of the impedance tensor in the inversion, but no tipper data were used because of the poor quality of the tipper data for a few sites, and we selected 13 periods, which are uniformly distributed with two periods per decade, of the data, from 0.001 to 1000 s. We tested several combinations of parameters in the process of computing a final inversion model (e.g., different cell sizes, initial models and error floors). For the final selected model that fits the data best and geologically plausible, we prepared a 3D mesh grid in which one site fell within a single cell of the 3D grid, and 1–3 cells exist between neighboring cells. The model space using the finite difference method was discretized in a rectangular grid having $80 \times 56 \times 42$ cells (including seven air layers) in x, y and z directions, respectively. Considering computational time and accuracy, cell sizes in the core region (80×50 km) were selected 1.4×1.4 km and increased laterally by a factor of 1.3 to cover 176×143 km area. In the vertical direction, the minimum cell sizes were 40 m, and cell sizes were increased with depth by a factor of 1.3. The base of the cells was at a depth of 997.5 km. The initial model (priori model as well) was chosen as a homogenous half space of 100 Ωm. The spatial smoothing parameters at every direction were chosen as 0.1 to find a reasonable model. The error floors of the impedances were set as 10% of $\sqrt{|Z_{xy} \times Z_{xy}|}$. We also tested different initial models (10 Ωm, 100 Ωm and 1000 Ωm), smoothing parameters (0.1, 0.2 and 0.3) and error floors (5%, 10% and 20%) and obtained quite similar inversion models. The initial RMS for final selected model shown in Fig. 4 was 8.22 and reduced to 3.6 after 23 iterations. Profile cross sections and representative depth sections extracted from 3D model are also shown in Figs. 5 and 6. The data fit for the final model is plotted in Fig. 7 as pseudo-sections of all components of the impedance tensor. As shown in Fig. 7, observed and calculated responses generally fit well.

Sensitivity tests

In order to examine the validity and spatial dimensions of the striking conductive features (C1 and C2) demonstrated in 3D model (Figs. 4, 5, 6), a set of tests were performed by using forward modeling in addition to multiple inversion runs including a range of starting models, grid discretization, data weighting and smoothing parameters. In this way, the sensitivity of the corresponding conductivity anomalies was tested to ensure that they are not artificially produced by inappropriate inversion implementations. Two main tests were conducted to examine the reliability of the deep conductive zones C1 and C2. For this purpose, a block with constant resistivity of 300 Ωm starting at four different depths 11.4 km (test-1), 19.36 km (test-2), 32.81 km (test-3) and 42.69 km (test-4) and terminating at the base of the model instead of the conductive zone C1 was introduced into the final selected 3D model in order to test the conductive zone C1, and a block with constant resistivity of 300 Ωm instead of the conductive zone C2 was also introduced into the final 3D model at four different depths, 14.86 km (test-1), 25.12 km (test-2), 32.81 km (test-3) and 42.69 km (test-4). To examine the sensitivity of impedance data against these inserted blocks, 3D forward modeling experiments were carried out. According to the forward responses shown in Fig. 8 for representative sites 122 and 148 located on top of the conductive zones C1 and C2, respectively, the existence of the resistive bodies in the 3D model has a significant impact on the data fits. By comparing the MT responses of the final 3D model with modified models, it can be suggested that MT data do not support the artificially inserted resistive bodies at corresponding depths. Therefore, the base of the conductive zones C1 and C2 imaged in 3D model is valid as a value approximately 45–50 km.

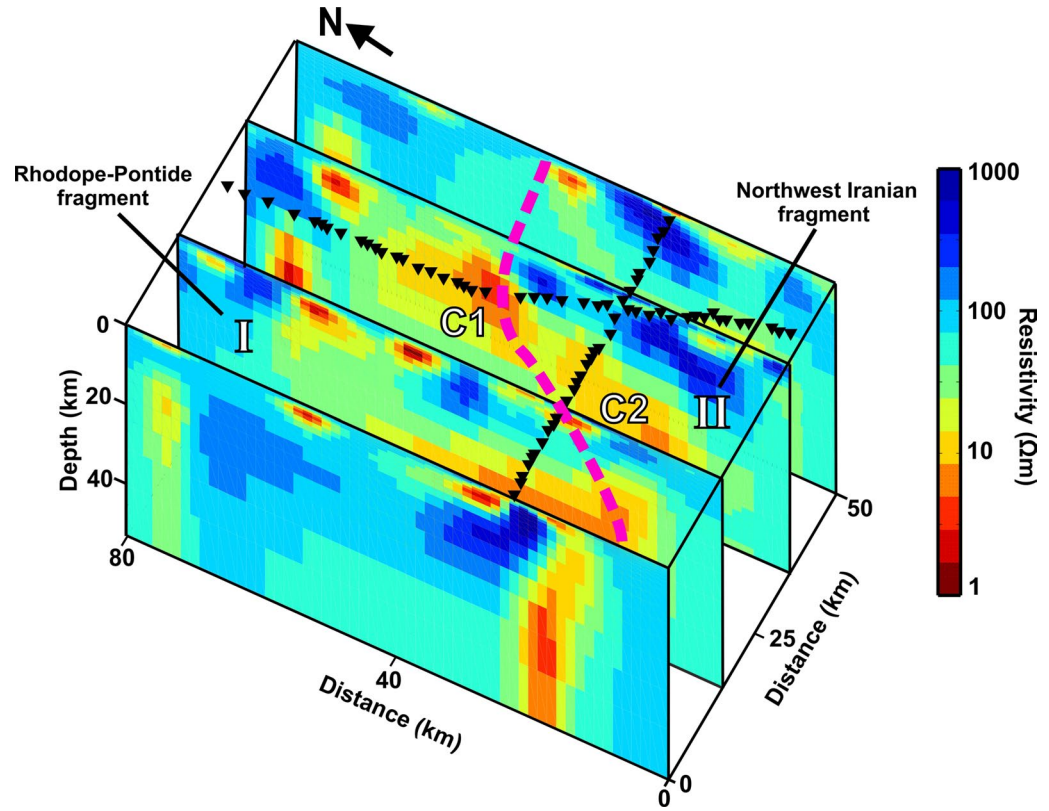

Fig. 4 3D perspective view displaying vertical north–south slices through the model and site locations at surface. The pink broken line displays the approximate boundary of the tectonic blocks (modified from Şengör et al. 2003), the Rhodope-Pontide and Northwest Iranian fragments. The conductive features C1 and C2 explained in the text

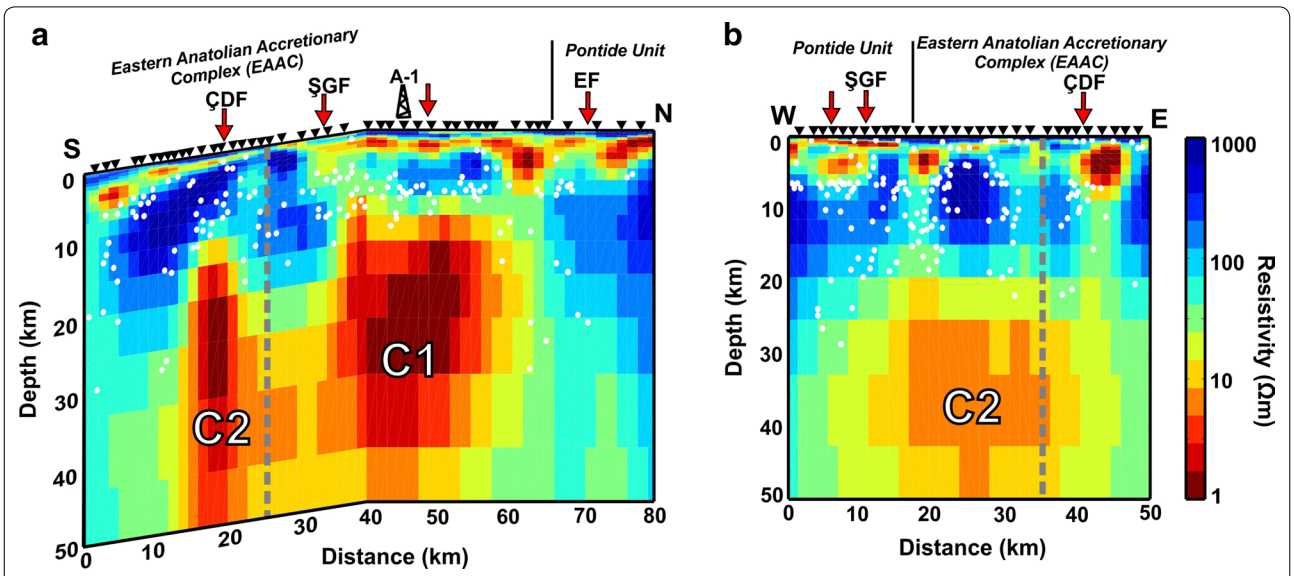

Fig. 5 G1 (**a**) and G2 (**b**) profile cross sections derived from 3D model. The surface trace of the faults (modified from Koçyiğit et al. 2001) is shown on the profiles as red arrows. The gray broken line represents the intersection of the profiles. The white dots indicate hypocenters of earthquakes. The earthquake hypocenters from 1900 to 2017 earthquake catalog prepared by the Kandilli Observatory and Earthquake Research Institute (KOERI) were projected onto profile cross sections. Earthquake hypocenters up to 35 km from the MT profiles were projected at right angles onto the cross sections

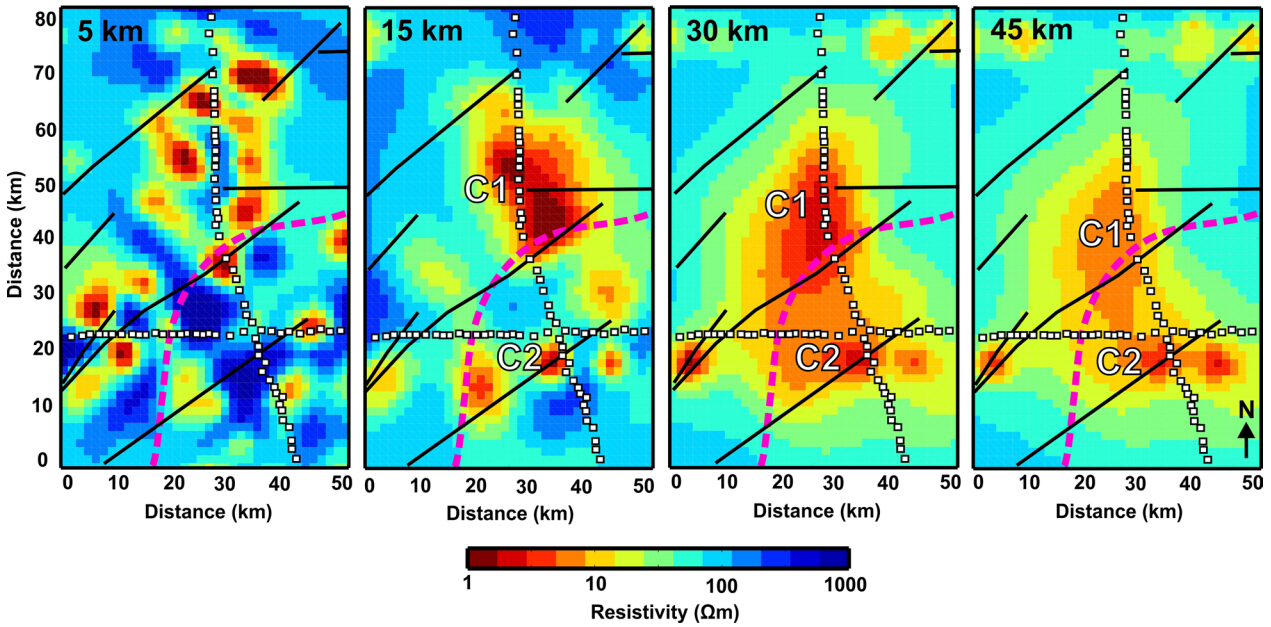

Fig. 6 Resistivity depth sections for different depths (5, 15, 30, 45 km), with projected surface trace of the faults (black solid lines), boundary of the tectonic blocks (pink broken lines), volcanic centers (red triangles) and station locations (white rectangulars)

Results and discussion

This study reveals the electrical conductivity structure of the intensely deformed east Anatolian Collision Zone beneath the EKP, northeastern Turkey, by using 3D inversion of the MT data. The most striking feature in the 3D model is the existence of mid-to-lower crustal conductive zones (C1 and C2) (Figs. 4, 5, 6). The conductive zones having high values of conductivity (~2–20 Ωm) begin to appear at a depth of 15–20 km in the crust of the EKP and disappear at depth below 45–50 km. The robustness of the corresponding anomalies was tested by sensitivity tests.

The conductive zones in the crust of the Earth are characterized by fluids with high ionic content, conducting minerals such as sulfide or graphite and partial melting, and these zones are influenced heavily by temperature and tectonic activity of the crust (Evans 2012). The conductive zones C1 and C2 with higher conductivities and its top at a depth of 15–20 km in the crust of the EKP may thus be associated with the thermal and tectonic state of the crust (Figs. 5, 6), and the electrical conductivity structure beneath the EKP can be utilized to constrain rheology of the crust.

Previous orogen-scale MT studies have revealed an electrical conductivity structure including a highly conductive mid-crustal zone that can be attributed to partial melts or partial melts, with coexisting aqueous fluids (Li et al. 2003; Unsworth et al. 2005; Türkoğlu et al. 2008; Rippe and Unsworth 2010; Unsworth 2010). In the study area, the high temperatures (1280 °C) at shallow depths (~45–50 km) and young volcanic activity implying a shallow magma chamber or mantle plume (Şengör 2001; Keskin 2005; Keskin et al. 2006) indicate that the mid-to-lower crustal conductive zones caused only by aqueous fluids are not possible at lower crustal depths, and thus, the presence of partial melting is a necessary argument for explaining the high conductivities in the crust of the EKP. Furthermore, fluids that could be released from the subducted slab together with increased heat flow may also lead to partial melting at mid-to-lower crustal depths as decreasing the melting point of the crust. The petrological data from collision-related volcanic units of the EKP provide evidence for partial melting (Keskin et al. 2006), and therefore, the crustal conductive zones at mid-to-lower crustal depths (15–45 km) can be attributed to zones of partial melting.

The presence of fluids in the crust of the earth is significant since it weakens the crust, and it may provide to characterize the regions where crustal flow could occur. The previous magnetotelluric studies in collision zones showed the fluid content of the crust and also associated the conductivity pattern with the possible crustal flow zones (Unsworth et al. 2004; Bai et al. 2010; Dong et al. 2016). The existence of highly conductive zones in the crust of the EKP may be an indication of rheologically weak zones where active deformation concentrated. On the other hand, compressional deformation in the region may cause the development of zones containing

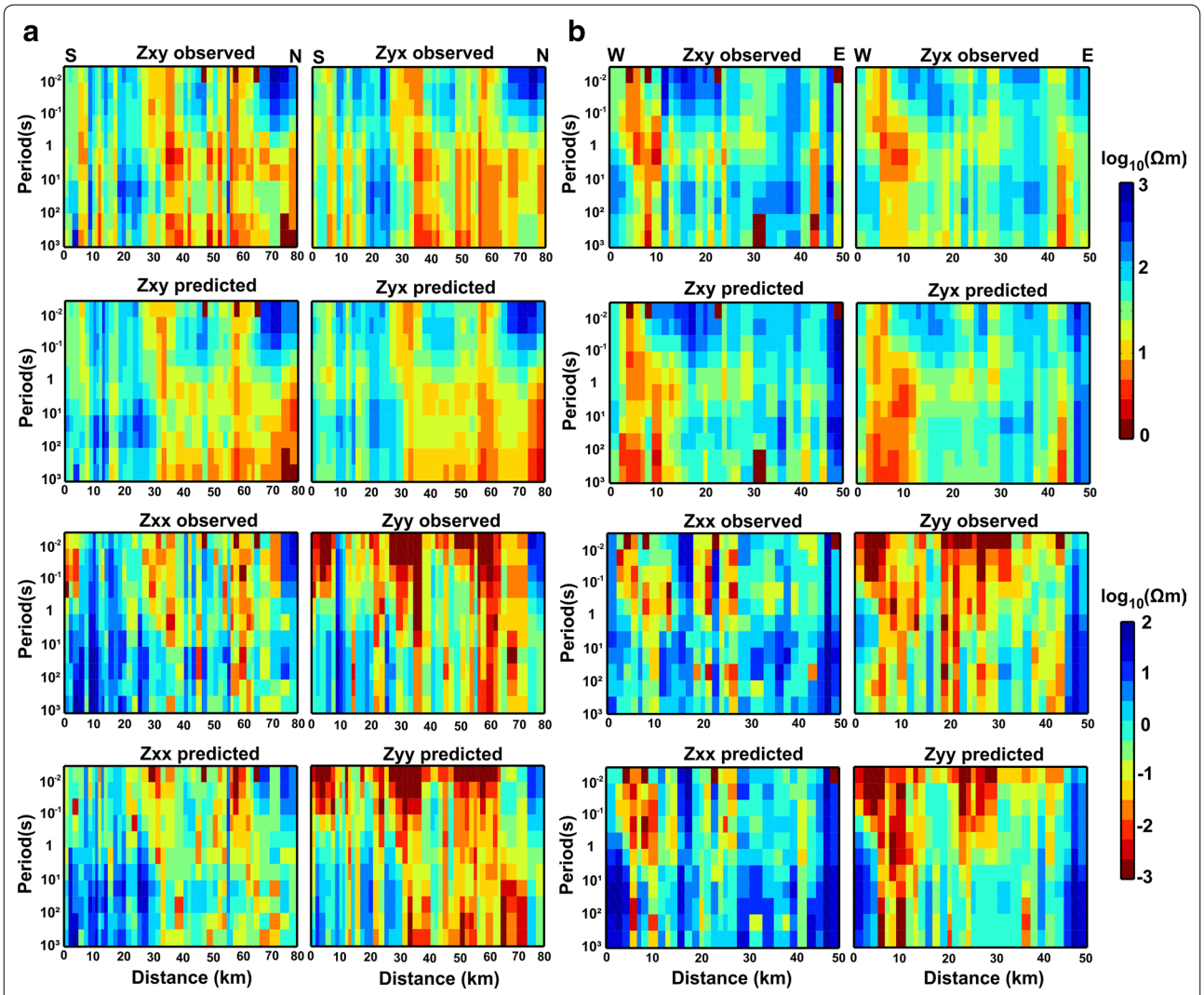

Fig. 7 Observed and predicted pseudo-sections of impedance tensor elements for G1 (**a**) and G2 (**b**) profiles

enhanced fluids through maintaining interconnected fluid paths between cracks. When the tectonic state of the region is taken into consideration, the mid-to-lower crustal conductive zones can be correlated with zone of deformation in the crust of EKP where direct convergence occurs between the Arabian and Eurasian Plates. Tullis et al. (1996) showed that interconnectivity increased with shear stress on deformed samples leads to a significant decrease in strength; therefore, it can be proposed that interconnection of fluids promoted by active deformation in the east Anatolian Collision Zone mechanically weakens the crust as a result of strain localization. The crust deforming by roughly north–south compression may lead to an increase in fluid content through maintaining fluid connection between cracks and thus lead to the generation of zones of fluid flow through the crust.

The very high conductivities in mid-to-lower crustal depths imply the presence of a low-percent partial melt in the crust, which is sufficient to produce an order of magnitude reduction in viscosity and represents a zone that is an order of magnitude weaker than the adjacent rocks (Unsworth et al. 2005). Beaumont et al. (2001) in their geodynamic models defined mid-to-lower crustal zones containing small amount of partial melt as melt weakening zones in the Tibetan Plateau, and they suggested that this amount of weakening is a required condition for strain localization and initiation of crustal flow in the collision zone. Therefore, it can be suggested that the amount of crustal melting inferred beneath the EKP is sufficient to reduce the strength of the crust needed

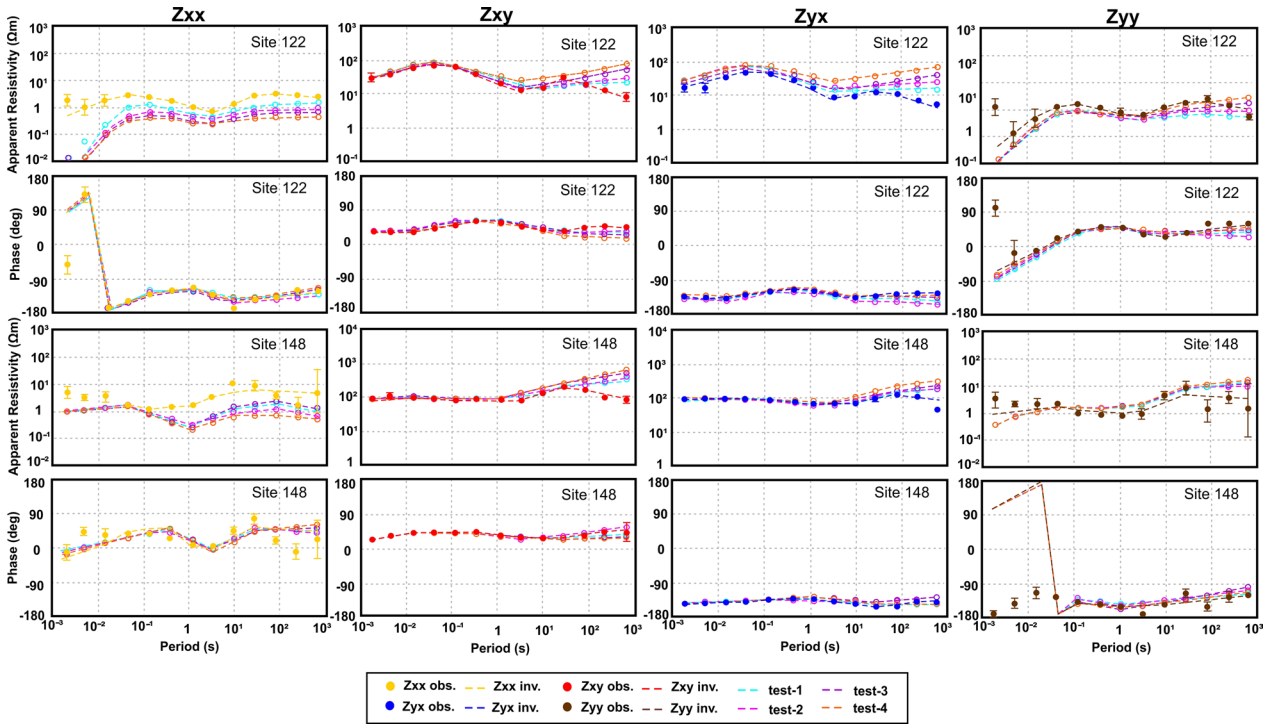

Fig. 8 MT sounding curves at two representative sites (122 and 148) for sensitivity tests with artificially inserted resistive bodies. The location of the sites is shown in Fig. 1b. The sites 122 and 148 are located above the conductive features C1 and C2, respectively

to allow crustal flow. Türkoğlu et al. (2008) in their 2D models presented the high-conductivity crustal zones by inverting the MT data obtained from two profiles perpendicular to the orogen (north–south) and proposed the presence of possible crustal flow zones in Eastern Anatolia. Unsworth (2010) also reviewed orogen-scale MT studies in his paper and suggested typical conductivity models characterizing a mid-crustal conductive zone with upper surface at 10–20 km for the collision zones. He proposed that if crustal flow exists in Eastern Anatolia, it must be in the orogen parallel east–west direction since the high-conductivity crustal zones in the Anatolian Plateau is not continuous in a north–south direction. The highly conductive zones presented in our 3D model also have similar characteristic and discrete property in north–south direction (Fig. 6). The results of our study in the EKP have confirmed the presence of the mid-to-lower crustal conductive zones detected by previous study in the Anatolian Plateau (Türkoğlu et al. 2008) and the characteristic conductivity model suggested by Unsworth (2010) for active continent–continent collision zones. In addition to that, in the present study, it has been shown the orogen parallel geometry of the conductive zones by analyzing the data in three dimensions, in particular by utilizing the data obtained from east–west-oriented MT profile (G2). According to that, the conductive zone C2 located in the intersection of two profiles shown by gray broken lines in Fig. 5 exhibits a vertical direction in the north–south direction (Fig. 5a), whereas it is much broader in the east–west direction (Fig. 5b). This geometry of the conductor (C2) may be a result of the roughly north–south-directed compressional tectonics of the region and an indication of the east–west-directed localized crustal flow at mid-to-lower crustal depths. In addition to that, when we compared our 3D model with the 2D model constructed from previous study for the Anatolian Plateau (profile E′-E) (Türkoğlu et al. 2008; Türkoğlu 2009) (Fig. 9), we may propose that crustal conductive zones in the lower crust spatially extend at least more than 100 km eastward beneath the northern part of the collision zone, which might be an indication of the presence of two localized crustal flow channels situated laterally parallel to the orogen and transporting crustal materials and shows that the electrical characteristic of the collision zone is continuous from west to east beneath the Anatolian Plateau. This direction of crustal flow is consistent with the direction of the compressional stresses associated with the collision of the Arabian plate with Eurasia (Reilinger et al. 1997). Therefore, based on the compressional tectonics and rheological heterogeneity of the crust, we may propose a model of nearly east–west-directed localized flow of the mid and lower

crust beneath the EKP. In this scenario, crust experiences roughly north–south-directed compressional stress and extensional stress perpendicular to the direction of the compression. The extensional stress may lead to the generation of the localized extensional zones and north–south-trending tensional cracks, characterizing weak areas in the lithosphere. By the northward subduction of the Arabian Plate beneath Eastern Anatolia, the hot upwelling materials may rise thorough these cracks to introduce the mid-to-lower crust, which lowers the viscosity locally and may cause east–west-directed localized crustal flow. The existing data alone cannot constrain the pattern of flow, from east to west or west to east. However, the direction of the compressional stresses associated with the collision of the Arabian plate with Eurasia together with the direction of geo-electric strike and the polarization directions of phase tensor ellipses indicate that the localized crustal flow may be in a nearly eastward or south–eastward direction with a very small angle which we may assume is eastward.

At shallow depths, the electrical conductivity structure is consistent with the surface geology and the surface expressions of past collision-related volcanism on the study area (Keskin et al. 1998; Koçyiğit et al. 2001; Keskin et al. 2006). The shallow conductive zones beneath the profiles can be correlated with Pliocene to Quaternary sediments deposited in the basins as a result of strike-slip mechanisms, and the resistive zones may be associated with Late Miocene to Quaternary collision-related volcanic units (Fig. 5). The samples obtained from the borehole A-1 (see Fig. 1b for location) also support the existence of these types of rocks (Fig. 10). Moreover, near surface zones of high conductivity are coincident with the strike-slip and normal faults of the EKP (Koçyiğit et al. 2001), as locating at the boundary of conductive zones, and the boundary of the Rhodope-Pontide and Northwest Iranian fragments is also clear at shallow depths (Fig. 6).

As shown in Fig. 5, the shallow and diffuse seismicity observed in the upper crust above and around the mid-to-lower crustal conductive zones (C1 and C2) implies that the crust is being actively deformed. This pattern of seismicity implies that the conductive zones that may include partial melt in the crust of the EKP are too weak to produce earthquake since such materials lead to the reduction in strength of the crust needed to permit the occurrence of the earthquakes. Furthermore, the seismicity around the conductive zones may be triggered by fluid infiltration from the conductive zones.

Conclusion

In this study, wideband MT data recorded by 74 sites at the EKP, northeastern Turkey, were analyzed and modeled. The TEM data acquired at the same locations were also utilized to correct for static shift on the MT data, and a borehole drilled inside the study area. For the first time, a 3D conductivity model of the east Anatolian Collision Zone around the EKP is presented. The model has provided a clear image of crustal structure in the study area and showed that the crustal conductivity beneath the EKP has a significant lateral variability with highly

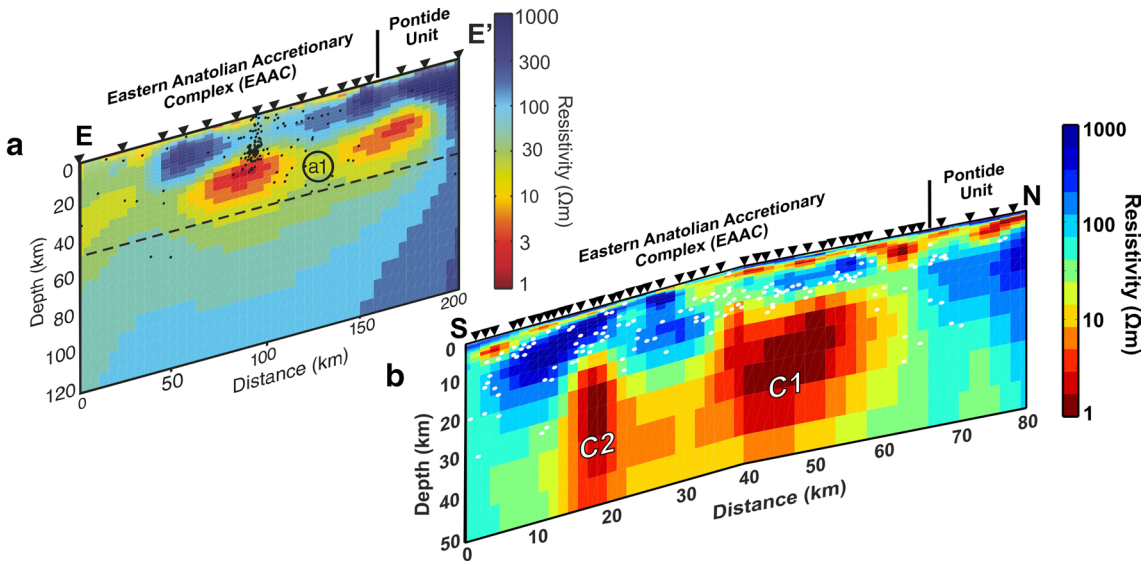

Fig. 9 Comparison of the geo-electric resistivity sections between profile E′-E from the previous 2D MT study (Türkoğlu et al. 2008; Türkoğlu 2009) (**a**) and the corresponding cross section from 3D MT interpretation (**b**)

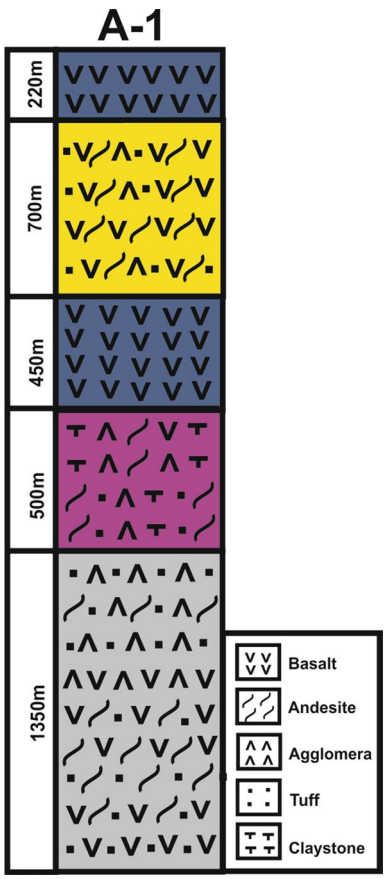

Fig. 10 Lithological section based on petrological analysis of rock samples from the borehole A-1 drilled in the EKP. The borehole reached a depth of more than 3 km, and it was drilled in 1999 by the Turkish Petroleum (TPAO). For borehole location, see Fig. 1b

conductive zones. The conductivity variations are attributed to rheological heterogeneity in the crust.

3D modeling of data allowed us to reveal that the crust of the collision zone appears to have two main mid-to-lower crustal conductive zones that are associated with local accumulations of melt. The electrical properties of these conductive zones characterize an elevated fluid content that is compatible with a weak crust, which may permit flow of crustal materials in the collision zone. The corresponding conductive zones have been previously identified further west of the collision zone, and in this study, it is shown that they extended horizontally to the east, which implies that the electrical characteristic of the collision zone is continuous from west to east beneath the Anatolian Plateau and may imply the existence of two localized crustal flow channels situated laterally parallel to the orogen. The roughly north–south compressional tectonics in the collision zone lead to the generation of north–south-trending tensional cracks perpendicular to the east–west-trending extension, which also supports the argument for east–west-directed localized mid-to-lower crustal flow.

These findings may be developed by utilizing a carefully designed 3D MT array in the collision zone and may provide new constraints on rheological properties of the crust. Furthermore, the results obtained from this study for east Anatolian Collision Zone may also support the idea that crustal flow can occur in the orogenic belts.

Abbreviations

1D: one-dimensional; 2D: two-dimensional; 3D: three-dimensional; EAAC: East Anatolian Accretionary Complex; ÇDF: Çobandede fault; EF: Erzurum fault; EKP: Erzurum–Kars Plateau; GB: Groom and Bailey decomposition; KOERI: Kandilli Observatory and Earthquake Research Institute; MT: Magnetotelluric; RMS: Root mean square; ŞGF: Şenkaya–Göle fault; TE: Transverse electric mode; TEM: Transient electromagnetic; TM: Transverse magnetic mode.

Authors' contributions

ÖH did major parts of the analyses of the study, performed the 3D inversion and drafted the manuscript. ATB has been advisor to the 3D inversion and preparation of the manuscript. ETÇ contributed to the 3D inversion. All authors read and approved the final manuscript.

Author details

[1] Geophysics Department, Kandilli Observatory and Earthquake Research Institute, Boğaziçi University, 34684 Çengelköy, Üsküdar, Istanbul, Turkey. [2] Geophysical Engineering Department, Faculty of Engineering, Karadeniz Technical University, 61080 Trabzon, Turkey. [3] Geophysical Engineering Department, Faculty of Engineering, Ankara University, 50. Yıl Yerleşkesi, H Blok, 06830 Gölbaşı, Ankara, Turkey.

Acknowledgements

We would like to thank Weerachai Siripunvaraporn for providing the 3D inversion code. We are also thankful for the contributions made by Erşan Türkoğlu and Gökhan Karcıoğlu. We are grateful to the editor and two reviewers for rigorous criticism and constructive comments, which helped us to improve the manuscript.

Competing interests

The authors declare that they have no competing interests.

Availability of data and materials

We used the data collected by Geosystem, UK, in August and September, 1998, on behalf of the Turkish Petroleum (TPAO).

Consent for publication

Not applicable.

Ethics approval and consent to participate

Not applicable.

Funding

The authors received no specific funding for this work.

Publisher's Note

Received: 23 February 2018 Accepted: 25 September 2018
Published online: 01 October 2018

References

Aitchison JC, Ali JR, Davis AM (2007) When and where did India and Asia collide? J Geophys Res 112:B05423. https://doi.org/10.1029/2006JB004706

Al-Damegh K, Sandvol E, Al-Lazki A, Barazangi M (2004) Regional seismic wave propagation (Lg–Sn) and Pn attenuation in the Arabian plate and surrounding regions. Geophys J Int 157:775–795. https://doi.org/10.1111/j.1365-246X.2004.02246.x

Al-Lazki A, Seber D, Sandvol E, Türkelli N, Mohamad R, Barazangi M (2003) Tomographic Pn velocity and anisotropy structure beneath the Anatolian plateau (eastern Turkey) and the surrounding region. Geophys Res Lett 30(24):8043. https://doi.org/10.1029/2003GL017391

Angus DA, Wilson DC, Sandvol E, Ni F (2006) Lithospheric structure of the Arabian and Eurasian collision zone in Eastern Turkey from S-wave receiver functions. Geophys J Int 166:1335–1346. https://doi.org/10.1111/j.1365-246X.2006.03070.x

Ateş A, Kearey P, Tufan S (1999) New gravity and magnetic anomaly maps of Turkey. Geophys J Int 136:499–502

Avşar U, Türkoğlu E, Unsworth M, Çağlar İ, Kaypak B (2013) Geophysical images of the North Anatolian Fault Zone in the Erzincan Basin, Eastern Turkey, and their tectonic implications. Pure appl Geophys 170:409–431. https://doi.org/10.1007/s00024-012-0521-5

Bai D, Unsworth MJ, Meju MA, Ma X, Teng J, Kong X, Sun Y, Wang L, Jiang C, Zhao C, Xiao P, Liu M (2010) Crustal deformation of the eastern Tibetan plateau revealed by magnetotelluric imaging. Nat Geosci 3:358–362. https://doi.org/10.1038/NGEO830

Barazangi M, Sandvol E, Seber D (2006) Structure and tectonic evolution of the Anatolian plateau in eastern Turkey. Geol Soc Am Spec Pap 409:463–474. https://doi.org/10.1130/2006.2409(22)

Beaumont C, Jamieson RA, Nguyen MH, Lee B (2001) Himalaya tectonics explained by extrusion of a low-viscosity crustal channel coupled to focused surface denudation. Nature 414:738–742. https://doi.org/10.1038/414738a

Booker J (2014) The magnetotelluric phase tensor: a critical review. Surv Geophys 35:7–40. https://doi.org/10.1007/s10712-013-9234-2

Bozkurt E (2001) Neotectonics of Turkey—a synthesis. Geodin Acta 14:3–30. https://doi.org/10.1080/09853111.2001.11432432

Caldwell TG, Bibby HM, Brown C (2004) The magnetotelluric phase tensor. Geophys J Int 158:457–469. https://doi.org/10.1111/j.1365-246X.2004.02281.x

Campanyà J, Ogaya X, Jones AG, Rath V, Vozar J (2016) The advantages of complementing MT profiles in 3-D environments with geomagnetic transfer function and interstation horizontal magnetic transfer function data: results from a synthetic case study. Geophys J Int 207:1818–1836. https://doi.org/10.1093/gji/ggw357

Dewey JF, Hempton MR, Kidd WSF, Şaroğlu F, Şengör AMC (1986) Shortening of continental lithosphere: the neotectonics of eastern Anatolia—a collision zone, in collision tectonics. Soc Spec Publ 19:3–36

Dong H, Wei W, Jin S, Ye G, Zhang L, Jing J, Yin Y, Xie C, Jones AG (2016) Extensional extrusion: insights into south-eastward expansion of Tibetan Plateau from magnetotelluric array data. Earth Planet Sci Lett 454:78–85

Evans RL (2012) Conductivity of earth materials. In: Chave AD, Jones AG (eds) The magnetotelluric method: theory and practice, 1st edn. Cambridge University Press, New York

Ferguson IJ, Jones AG, Chave AD (2012) Case histories and geological applications. In: Chave AD, Jones AG (eds) The magnetotelluric method: theory and practice, 1st edn. Cambridge University Press, New York

Gamble T, Goubau WM, Clarke J (1979) Magnetotellurics with a remote magnetic reference. Geophysics 44(1):53–68

Gök R, Pasyanos M, Zor E (2007) Lithospheric structure of the continent–continent collision zone: eastern Turkey. Geophys J Int 169(3):1079–1088. https://doi.org/10.1111/j.1365-246X.2006.03288.x

Groom RW, Bailey RC (1989) Decomposition of magnetotelluric impedance tensors in the presence of local three-dimensional galvanic distortion. J Geophys Res Solid Earth 94(B2):1913–1925

Innocenti F, Mazzuoli R, Pasquare G, Radicati di Brozolo F, Villari L (1982) Tertiary and quaternary volcanism of the Erzurum–Kars area (Eastern Turkey): geochronological data and geodynamic evolution. J Volcanol Geotherm Res 13:223–240. https://doi.org/10.1016/0377-0273(82)90052-X

Jones AG (2012) Distortion of magnetotelluric data: its identification and removal. In: Chave AD, Jones AG (eds) The magnetotelluric method: theory and practice, 1st edn. Cambridge University Press, New York

Keskin M (2003) Magma generation by slab steepening and breakoff beneath a subduction-accretion complex: an alternative model for collision-related volcanism in eastern Anatolia, Turkey. Geophys Res Lett 30(24):8046. https://doi.org/10.1029/2003GL018019

Keskin M (2005) Domal uplift and volcanism in a collision zone without a mantle plume: evidence from Eastern Anatolia. http://www.mantleplumes.org/Anatolia.html. Accessed 3 Jan 2018

Keskin M, Pearce JA, Mitchell JG (1998) Volcano-stratigraphy and geochemistry of collision-related volcanism on the Erzurum–Kars Plateau, Northeastern Turkey. Volcanol Geotherm Res 85:355–404

Keskin M, Pearce JA, Kempton PD, Greenwood P (2006) Magma–crust interactions and magma plumbing in a post-collision setting: geochemical evidence from the Erzurum–Kars Volcanic Plateau, Eastern Turkey. Geol Soc Am Spec Pap 409:475–505. https://doi.org/10.1130/2006.2409(23)

Koçyiğit A, Yılmaz A, Adamia S, Kuloshvili S (2001) Neotectonics of East Anatolian Plateau (Turkey) and Lesser Caucasus: implications for transition from thrusting to strike-slip faulting. Geodin Acta 14:177–195

Krieger L, Peacock JR (2014) MTpy: a Python toolbox for magnetotellurics. Comput Geosci 72:167–175. https://doi.org/10.1016/j.cageo.2014.07.013

Larsen JC, Mackie RL, Manzella A, Fiordelisi A, Rieven S (1996) Robust smooth magnetotelluric transfer functions. Geophys J Int 124:801–819

Ledo J, Queralt P, Pous J (1998) Effects of galvanic distortion on magnetotelluric data over a three-dimensional regional structure. Geophys J Int 132:295–301

Li S, Unsworth MJ, Booker JR, Wei W, Tan H, Jones AG (2003) Partial melt or aqueous fluid in the mid-crust of Southern Tibet? Constraints from INDEPTH magnetotelluric data. Geophys J Int 153:289–304

Maggi A, Priestley K (2005) Surface waveform tomography of the Turkish–Iranian plateau. Geophys J Int 160:1068–1080. https://doi.org/10.1111/j.1365-246X.2005.02505.x

McKenzie DP (1972) Active tectonics of the Mediterranean region. Geophys J R Astron Soc 30:109–185. https://doi.org/10.1111/j.1365-246X.1972.tb02351.x

McNeice GW, Jones AG (2001) Multisite, multifrequency tensor decomposition of magnetotelluric data. Geophysics 66(1):158–173

Örgülü G, Aktar M, Türkelli N, Sandov E, Barazangi M (2003) Contribution to the seismotectonics of Eastern Turkey from moderate and small size events. Geophys Res Lett 30(24):8040. https://doi.org/10.1029/2003GL018258

Patro KP, Egbert GD (2011) Application of 3D inversion to magnetotelluric profile data from Deccan Volcanic Province of Western India. Phys Earth Planet Inter 184:33–46. https://doi.org/10.1016/j.pepi.2011.04.005

Pearce JA, Bender JF, De Long SE, Kidd WSF, Low PJ, Güner Y, Şaroğlu F, Yılmaz Y, MoorbathS Mitchell JG (1990) Genesis of collision volcanism in eastern Anatolia, Turkey. J Volcanol Geoth Res 44:189–229

Pellerin L, Hohmann GW (1990) Transient electromagnetic inversion: a remedy for magnetotelluric static shifts. Geophysics 55:1242–1250. https://doi.org/10.1190/1.1442940

Reilinger R, McClusky SC, Oral MB, King RW, Toksoz MN (1997) Global positioning system measurements of present-day crustal movements in the Arabia–Africa–Eurasia plate collision zone. J Geophys Res 102:9983–9999

Reilinger R, McClusky S, Vernant P, Lawrence S, Ergintav S, Çakmak R, Özener H, Kadirov F, Guliev I, Ruben S, Nadariya M, Hahubia G, Mahmoud S, Sakr K, ArRajehi A, Paradisis D, Al- Aydrus A, Priilepin M, Guseva T, Evren E, Dmitrotsa A, Filikov SV, Gomez F, Al-Ghazzi R, Karam G (2006) GPS constraints on continental deformation in the Africa–Arabia–Eurasia continental collision zone and implications for the dynamics of plate interactions. J Geophys Res 111:B05411. https://doi.org/10.1029/2005JB004051

Rippe D, Unsworth M (2010) Quantifying crustal flow in Tibet with magnetotelluric data. Phys Earth Planet Inter 179:107–121. https://doi.org/10.1016/j.pepi.2010.01.009

Rotstein Y, Kafka AL (1982) Seismotectonics of the southern boundary of Anatolia, eastern Mediterranean region, subduction, collision and arc jumping. J Geophys Res 87:7694–7706. https://doi.org/10.1029/JB087iB09p07694

Şengör AMC (2001) Elevations as indicator of mantle-plume activity. Boulder Colo Geol Soc Am Spec Pap 352:183–225. https://doi.org/10.1130/0-8137-2352-3.183

Şengör AMC, Kidd WSF (1979) Post-collisional tectonics of the Turkish–Iranian Plateau and a comparison with Tibet. Tectonophysics 55:361–376. https://doi.org/10.1016/0040-1951(79)90184-7

Şengör AMC, Yılmaz Y (1981) Tethyan evolution of Turkey: a plate tectonic approach. Tectonophysics 75:181–241. https://doi.org/10.1016/0040-1951(81)90275-4

Şengör AMC, Özeren S, Genç T, Zor E (2003) East Anatolian high plateau as a mantle-supported, N-S shortened domal structure. Geophys Res Lett 30(24):8045. https://doi.org/10.1029/2003GL017858

Siripunvaraporn W, Egbert G, Lenbury Y, Uyeshima M (2005a) Three-dimensional magnetotelluric: data-space method. Phys Earth Planet Inter 150:3–14. https://doi.org/10.1016/j.pepi.2004.08.023

Siripunvaraporn W, Egbert G, Uyeshima M (2005b) Interpretation of two-dimensional magnetotelluric profile data with three-dimensional inversion: synthetic examples. Geophys J Int 160:804–814. https://doi.org/10.1111/j.1365-246X.2005.02527.x

TEMIX XL v.4 (1996) Users manual: transient electromagnetic data interpretation software. Interpex Ltd., Golden, Colo

Tullis J, Yund R, Farver J (1996) Deformation enhanced fluid distribution in feldspar aggregates and implications for ductile shear zones. Geology 24:63–66

Türkelli N, Sandvol E, Zor E, Bekler T, Al-Lazki A, Karbulut H, Kuleli S, Eken T, Gürbüz C, Bayraktutan S, Seber D, Barazangi M (2003) Seismogenic zones in Eastern Turkey. Geophys Res Lett 30(24):8039. https://doi.org/10.1029/2003GL018023

Türkoğlu E (2009) A magnetotelluric investigation of the Arabia–Eurasia collision in Eastern Anatolia. PhD thesis

Türkoğlu E, Unsworth M, Çağlar İ, Tuncer V, Avşar Ü (2008) Lithospheric structure of the Arabia–Eurasia collision zone in eastern Anatolia: magnetotelluric evidence for widespread weakening by fluids? Geology 36:619–622. https://doi.org/10.1130/G24683A

Türkoğlu E, Unsworth M, Bulut F, Çağlar İ (2015) Crustal structure of the North Anatolian and East Anatolian Fault Systems from magnetotelluric data. Phys Earth Planet Inter 241:1–14

Unsworth M (2010) Magnetotelluric studies of active continent–continent collisions. Surv Geophys 31:137–161. https://doi.org/10.1007/s10712-009-9086-y

Unsworth M, Wei W, Jones AG, Li S, Bedrosian P, Booker J, Sheng J, Ming D, Handong T (2004) Crustal and upper mantle structure of the northern Tibet imaged with magnetotelluric data. J Geophys Res 109:B02403. https://doi.org/10.1029/2002JB002305

Unsworth M, Jones AG, Wei W, Marquis G, Gokarn S, Spratt JE, INDEPTH-MT team (2005) Crustal rheology of the Himalaya and southern Tibet inferred from magnetotelluric data. Nature 438:78–81. https://doi.org/10.1038/nature04154

Yılmaz Y, Tüysüz O, Yiğitbaş E, Genç ŞC, Şengör AMC (1997) Geology and tectonic evolution of the Pontides. In: Robinson AG (ed) Regional and petroleum geology of the Black Sea and surrounding region, AAPG Memoir 68:183–226